Nanostructures

DOI: 10.1002/ange.201303480

Hierarchical Nanosheet-Based MoS_2 Nanotubes Fabricated by an Anion-Exchange Reaction of MoO_3–Amine Hybrid Nanowires**

*Sifei Zhuo, You Xu, Weiwei Zhao, Jin Zhang, and Bin Zhang**

Dedicated to Professor Helmuth Möhwald

Since the discovery of carbon nanotubes in 1991,[1] great effort has been directed toward the development of advanced methods for the fabrication of various types of nanotubes as a result of their unique physical/chemical properties as well as their potential applications in a variety of fields. Novel applications of fullerene-like MoS_2 in catalysts,[2,3] transistors,[4] lubricants,[5] hydrogen storage,[6] batteries[7] and supercapacitors[8] are driving the exploration of synthetic approaches that enable control of its structure and morphology.[2–9] For example, well-designed MoS_2-based composite catalysts for an efficient hydrogen-evolution reaction (HER) were described by the Chorkendorff research group.[3a,b] Hu and co-workers successfully developed amorphous molybdenum sulfide films as highly effective electrocatalysts for HER.[3f,g] Among the various structures, MoS_2 nanotubes were first synthesized by Tenne and co-workers[10] by the gas reaction of MoO_{3-x} and H_2S under a reducing atmosphere at elevated temperatures (800–950 °C). However, the current methods for the preparation of MoS_2 nanotubes always require high temperatures or dangerous gases, including H_2 and H_2S, and a complicated procedure. Furthermore, hierarchical nanosheet-based MoS_2 nanotubes have rarely been reported, especially for enhanced photoelectrochemical HER.

Since the discovery of the cation-exchange reaction of inorganic nanocrystals by the Alivisatos research group,[11] much attention has been paid to the conversion of one inorganic crystalline material into another through this cation-exchange method. Further developments in the cation-exchange reaction also enable the production of nanoporous structures with adjustable composition.[12,13] Very recently, inorganic–organic hybrid precursors were found to be efficient precursors for the production of porous or tubular inorganic materials.[14] By using inorganic–organic hybrid nanosheets as the starting materials, we developed a facile cation-exchange strategy for the preparation of nanoporous single-crystal-like $Cd_xZn_{1-x}S$ nanosheets[15a] and hollow $Cd_xZn_{1-x}Se$ nanoframes.[15b] Hierarchical nanostructures have attracted increasing attention owing to their improved catalytic properties.[16] Despite these advances in the production of porous and tubular nanostructures, the anion-exchange synthesis of hierarchical nanosheet-based nanotubes still remains challenging.

Herein, we present a facile strategy for the synthesis of hierarchical nanosheet-based 2H-MoS_2 nanotubes by an anion-exchange reaction of the inorganic–organic hybrid $Mo_3O_{10}(C_2H_{10}N_2)$ (ethylenediamine trimolybdate, named MoO_3–EDA herein) nanowires with L-cysteine at elevated temperature. The dissolution of ethylenediamine (EDA) in the solvent and the concentration-gradient-driven outward diffusion of MoO_3–EDA during the anion-exchange reaction were found to play a key role in the formation of the hierarchical nanosheet-based nanotubes. Furthermore, the as-prepared hierarchical nanosheet-based MoS_2 nanotubes are highly active for electrochemical and photoelectrocatalytic HER through water splitting under visible-light illumination.

The inorganic–organic MoO_3–EDA hybrid nanowires were synthesized by a method reported by Tang and co-workers.[17] The as-prepared products were first examined by scanning electron microscopy (SEM) and X-ray diffraction (XRD). Typical SEM images (Figure 1 a,b) clearly show that the MoO_3–EDA nanowires were synthesized successfully in high yields with lengths of about 5–10 μm. The XRD pattern (Figure 1 c) identified these hybrid precursors as $Mo_3O_{10}(C_2H_{10}N_2)$ (named MoO_3–EDA herein; ICDD: 00-058-1318). The Fourier transform infrared transmission (FTIR) spectrum (see Figure S1 in the Supporting Information) indentified these as-prepared precursors as inorganic–organic hybrids, and line-scan electron energy loss spectroscopy (EELS; Figure 1 d) further illustrated the uniform distribution of the elements Mo, O, C, and N in the nanowires and thus suggested that the nanowire precursors were composed of Mo, O, C, and N.

The anion-exchange reaction for the transformation of the MoO_3–EDA nanowires was carried out by heating an aqueous solution of the hybrid nanowires as precursors and L-cysteine as the sulfur source at 200 °C for 14 h. Upon the reaction of the hybrid precursors with the S^{2-} anions, which were present in excess, the solid nanowires became hierarchical nanosheet-based 1D nanostructures with the retention of their macroscopic one-dimensional morphology (Figure 1 e,f). High-magnification SEM images (Figure 1 f,g; see also Figure S2a in the Supporting Information) revealed that the

[*] S. Zhuo,[+] Y. Xu,[+] W. Zhao, J. Zhang, Prof. Dr. B. Zhang
Department of Chemistry, School of Science, Tianjin University and The Co-Innovation Center of Chemistry and Chemical Engineering of Tianjin
Tianjin 300072 (China)
E-mail: bzhang@tju.edu.cn

[+] These authors contributed equally.

[**] This research was supported financially by the National Natural Science Foundation of China (No. 20901057 and No. 11074185), the National Basic Research Program of China (2009CB939901), and the Innovation Foundation of Tianjin University.

Supporting information for this article is available on the WWW under http://dx.doi.org/10.1002/anie.201303480.

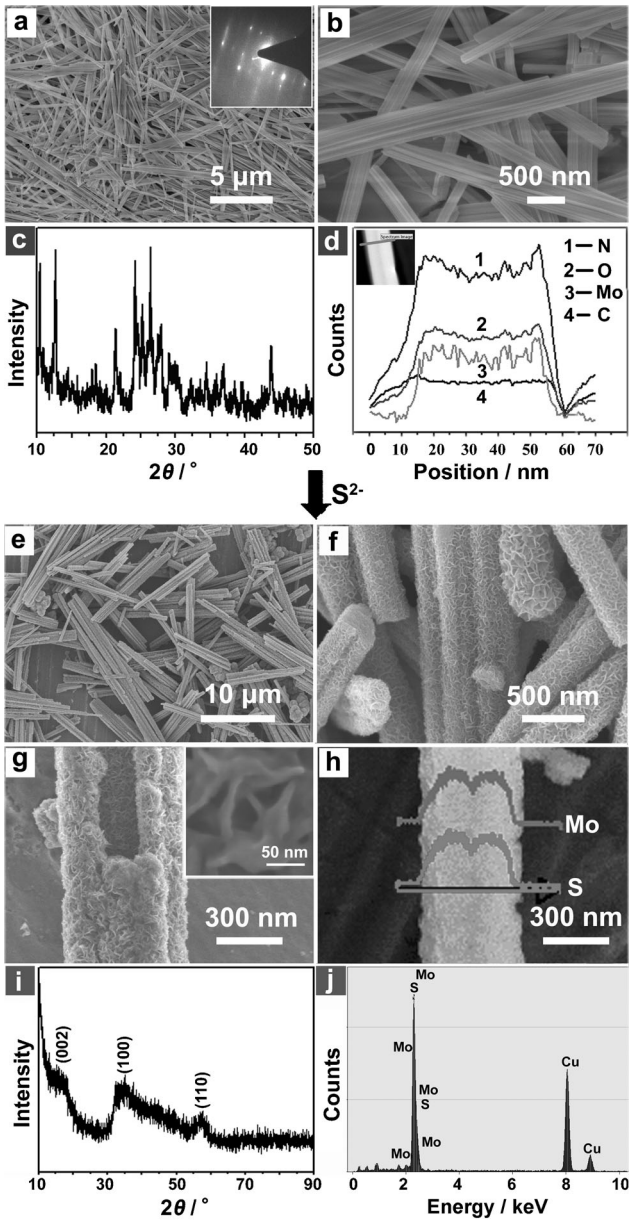

Figure 1. a,b) SEM images, c) XRD pattern, and d) line-scan EELS elemental distributions of the MoO_3–EDA hybrid nanowires. e–g) SEM images, h) line-scan SEM elemental distributions, i) XRD pattern, and j) point-scan EDX spectrum of the hierarchical nanosheet-based MoS_2 nanotubes. The inset in (d) is the image to indicate the position to obtain the line-scan EELS profile.

products of this anion-exchange reaction are composed of nanosheets with a thickness of less than 10 nm. The SEM image in Figure 1 g and the associated line-scan energy-dispersive X-ray (EDX) profile (Figure 1 h) clearly show the tubular character of these products, and thus indicate that the products are hierarchical nanosheet-based nanotubes. These nanostructures were assigned to the hexagonal phase of 2H-MoS_2 (JCPDS 37-1492) on the basis of the XRD pattern (Figure 1 i). Moreover, the visible (002) diffraction peak indicates the formation of a well-stacked layered structure of MoS_2 during the hydrothermal process. The point-scan EDX spectrum (Figure 1 j) further confirmed the composition of the products as MoS_2. The FTIR spectra of the starting materials and products also confirmed that the hybrid precursors had been transformed into inorganic materials (see Figure S1 in the Supporting Information). These results imply that the anion-exchange reaction of the MoO_3–EDA hybrid nanowires with sulfur anions successfully leads to the formation of hierarchical nanosheet-based MoS_2 inorganic nanotubes.

The morphology and structure of the hierarchical nanosheet-based MoS_2 nanostructures were further characterized by transmission electron microscopy (TEM), high-resolution TEM (HRTEM), and selected-area electron diffraction (SAED). Typical TEM images (Figure 2 a; see also Figure S2b

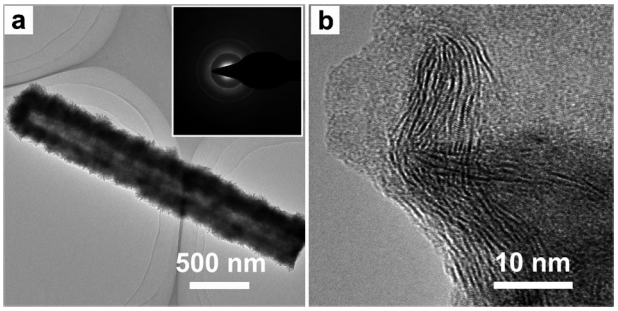

Figure 2. a) TEM image and b) HRTEM image of a hierarchical nanosheet-based MoS_2 nanotube. The inset in (a) is the SAED pattern of an individual nanosheet.

in the Supporting Information) reveal the tubular architecture of the hierarchical nanosheet-based MoS_2 nanostructures, which have an internal diameter of about 200 nm. The SAED pattern (see the inset in Figure 2 a) and HRTEM image (Figure 2 b) confirm that the units of the as-synthesized hierarchical nanotubes are polycrystalline nanosheets. The HRTEM image also demonstrates the well-stacked layered structure of MoS_2, with an interlayer distance of 0.62 nm. Moreover, the pore-size distributions (see Figure S3 in the Supporting Information) suggest that the MoS_2 nanotubes contain macropores of around 200 nm in diameter and mesopores with a diameter of about 30 nm. On the basis of the SEM and TEM images, these macropores are thought to result from the tubular structure, and the mesopores originate from the interspaces between MoS_2 nanosheets. Furthermore, scanning transmission electron microscopy (STEM) elemental mapping images (see Figure S4 in the Supporting Information) indicated the uniform distribution of Mo and S in the as-prepared hierarchical MoS_2 nanotubes. These results further demonstrate that the hierarchical nanosheet-based MoS_2 nanotubes can be synthesized successfully by introducing S^{2-} anions into inorganic–organic hybrid MoO_3–EDA nanowires through an anion-exchange reaction.

To gain insight into the chemical transformation mechanism underlying the generation of the hierarchical nanosheet-based MoS_2 nanotubes by the anion-exchange reaction, we used SEM, TEM, and STEM elemental distribution to

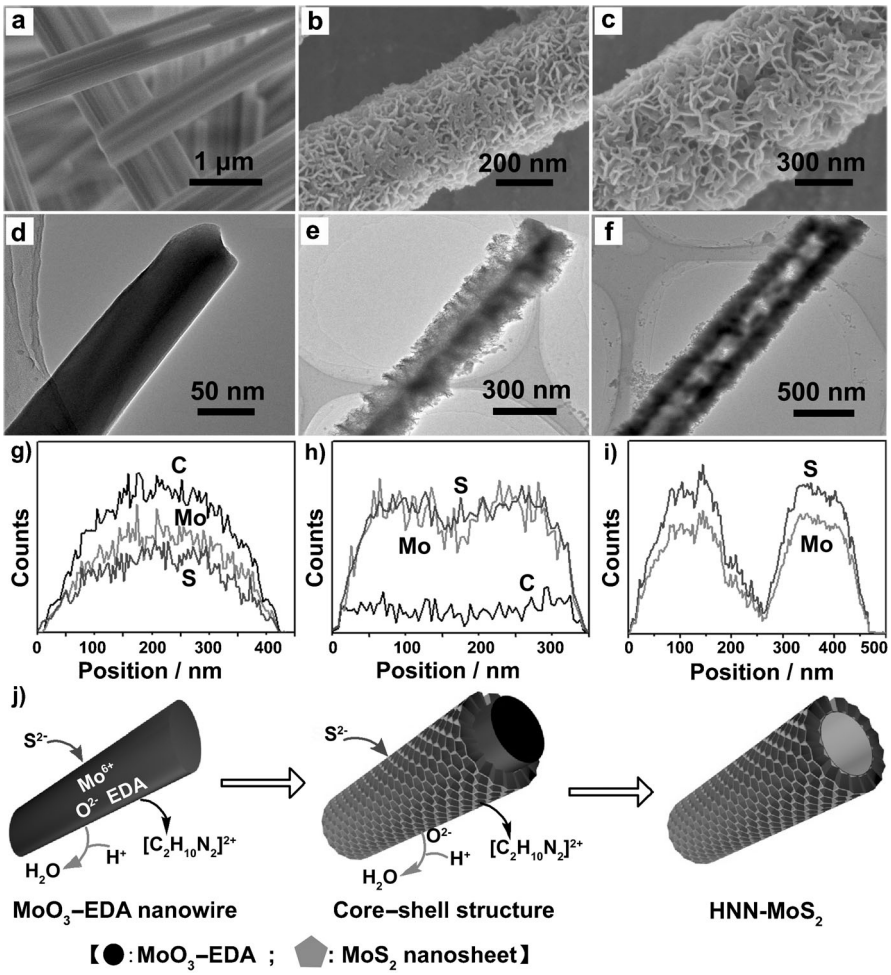

Figure 3. a–c) SEM images, d–f) TEM images, and g–i) line-scan STEM elemental distributions of the intermediates collected after the anion-exchange reaction had proceeded for 0 h (a,d), 6 h (b,e,g), 8 h (h), and 12 h (c,f,i). j) Schematic representation of the synthesis of hierarchical nanosheet-based MoS_2 nanotubes (HNN-MoS_2; cross-section view) through the anion-exchange reaction of the inorganic–organic MoO_3–EDA hybrid nanowires with S^{2-} at elevated temperature.

examine intermediates collected at different stages of the reaction. Figure 3 depicts the morphological evolution of the hierarchical nanosheet-based nanotubes from the solid hybrid nanowires. When the anion-exchange reaction is carried out for 6 h, the outer surface of the hybrid nanowires becomes rough and encompasses numerous voids within the nanosheets (Figure 3 b,e; Figure 3 a,d shows the initial hybrid nanowires for comparison), whereas the internal part of the intermediates remains a solid inorganic–organic hybrid (Figure 3 e). The line-scan EDX profile (Figure 3 g) also confirms that the reaction intermediates after 6 h are solid hybrid nanowires with a rough outer surface composed of porous nanosheets. When the reaction was continued for a longer period, the bimodal distribution of Mo and S in the line-scan EDX profiles appeared at 8 h (Figure 3 h), and the signals of C and O slowly decreased to become negligible at 8 h (Figure 3 g,h). These EDX profiles reveal the formation of inorganic tubular MoS_2 through the outward diffusion of Mo and the following reaction with sulfur anions, as well as the dissolution of the organic EDA component of the hybrid wirelike precursors. A prolonged reaction time for the transformation finally led to the generation of hierarchical nanosheet-based MoS_2 nanotubes (Figure 3 c,f,i).

On the basis of these results, we propose that the mechanism for the transformation of MoO_3–EDA inorganic–organic hybrid nanowires into hierarchical nanosheet-based MoS_2 nanotubes involves an anion-exchange reaction of the hybrid nanowires and outward diffusion of the inner hybrid MoO_3–EDA, as well as the dissolution of EDA in water (Figure 3 j). First, S^{2-} anions formed by the breakdown of L-cysteine at elevated temperature slowly exchange with O^{2-} anions of MoO_3–EDA to form MoS_3 at the surface of the hybrid nanowires, and this MoS_3 is quickly reduced to MoS_2.[19] O^{2-} anions react with hydrogen cations derived from the dissociation of L-cysteine to produce H_2O. The unique layered structure of MoS_2 and the dissolution of EDA ensure the formation of porous MoS_2 nanosheets at the surface of the solid wirelike precursors (Figure 3 b,e,g). In the following process, the outward diffusion of the internal MoO_3–EDA to the outer surface of the starting one-dimensional (1D) materials, as driven by the concentration gradient of MoO_3–EDA,[14a] provides a source of MoO_3 for further anion exchange and the growth of the MoS_2 nanosheets. The continuous outward diffusion of internal MoO_3–EDA results in the appearance of a hollow region inside the starting 1D materials and some channels on the walls of these materials. When the MoO_3–EDA component has been completely transformed into MoS_2, a transformation that accompanies the dissolution of EDA in the solvent, the inner hollow regions become hollow tubes. Finally, kinetically stable nanosheet-based hierarchical MoS_2 nanotubes are obtained. The hierarchical nanosheet-based MoS_2 nanotubes could only be obtained when inorganic–organic hybrid nanowires were used as the starting materials. When inorganic MoO_3 nanowires[18] were used in place of the MoO_3–EDA hybrid nanowires under otherwise unchanged conditions, the products of anion exchange were particle-like aggregates of MoS_2 sheets with microscale dimensions rather than nanosheet-based nanotubes (see Figure S5 in the Supporting Information). This result also reveals that the presence of the organic component EDA is significant for the synthesis of nanosheet-based nanotubes. Our preliminary hypothesis is that the continuous dissolution of EDA in the solvent is helpful for the outward diffusion of MoO_3 and the formation of the hierarchical

porous structures. Furthermore, it was found that the anion exchange is independent of the sulfur source. For example, the reaction of the MoO_3–EDA hybrid nanowires with thiourea or thiacetamide instead of cysteine under the same conditions also led to the formation of hierarchical nanosheet-based MoS_2 nanotubes (see Figure S6 in the Supporting Information).

Recently, transition-metal dichalcogenides with a layered structure demonstrated intriguing efficiency in the conversion of solar into electric energy and remarkable stability to photocorrosion in a photoelectrolysis cell.[20] In this study, we tested photoelectrocatalytic hydrogen generation by water splitting in comparative studies of the catalytic activity of the as-prepared hierarchical nanosheet-based MoS_2 nanotubes (HNN-MoS_2) and commercial MoS_2 samples (C-MoS_2; see Figure S7 in the Supporting Information). UV/Vis diffuse reflectance spectra (Figure 4a) showed that HNN-MoS_2

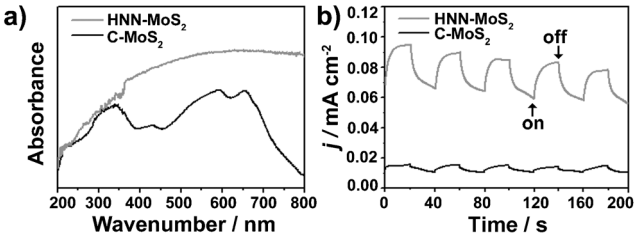

Figure 4. a) UV/Vis diffuse reflectance spectra and b) photocurrent-density response at an applied bias of 0.6 V versus SCE under visible-light illumination ($\lambda > 420$ nm) of the as-prepared hierarchical MoS_2 nanotubes (HNN-MoS_2) and commercial MoS_2 samples (C-MoS_2).

exhibits a broad and continuous photoabsorption range from 420 to 800 nm, which matches the energy bandgap of multilayered polycrystalline MoS_2.[20] Furthermore, HNN-MoS_2 has a stronger absorption ability and a wider adsorption region than C-MoS_2. Figure 4b displays the photocurrent-density responses of HNN-MoS_2 and C-MoS_2 at an applied bias of 0.6 V versus the saturated calomel reference electrode (SCE) during repeated on/off cycles of visible-light illumination ($\lambda > 420$ nm) in the presence of lactic acid[3d] (10 vol%) as an electron donor. The photocurrent response of HNN-MoS_2 was prompt, steady, and reproducible, and the short-circuit photocurrent density was 0.09 mA cm^{-2} (ca. 0.67 mA mg^{-1}), which is nearly 9 times higher than that of C-MoS_2 (Figure 4b). Moreover, the amplitude of the oscillations of HNN-MoS_2 (about 0.026 mA cm^{-2}) was nearly 6 times than that observed for C-MoS_2 (0.0045 mA cm^{-2}), which indicates that HNN-MoS_2 is much more sensitive than C-MoS_2 to visible light. These results reveal that the hydrogen-release rate of HNN-MoS_2 is approximately 9 times higher than that of C-MoS_2. In comparison with C-MoS_2, HNN-MoS_2 has many more edges exposed to the solution; these edges have been identified as active sites[21] for electrochemical H_2 evolution. HNN-MoS_2 was also found to be highly stable under visible-light illumination (see Figure S8b in the Supporting Information). Thus, the as-prepared HNN-MoS_2 is one of the most promising materials for photoelectrocatalytic hydrogen evolution. Electrochemical impedance spectroscopy (EIS; see Figure S9 in the Supporting Information) indicated that the photoelectrochemical water-splitting kinetics of the HNN-MoS_2 electrodes involve a charge-transfer process at the electrode/electrolyte interface and the diffusion of charges inside the electrode. The latter may be caused by the unique hierarchical porous structure of HNN-MoS_2. The improved activity of HNN-MoS_2 may be attributed to an enhanced ability to absorb photons and the unique hierarchical porous tubular structure of the nanosheets. Our preliminary results also reveal that the as-prepared HNN-MoS_2 exhibits better activity towards the electrochemical HER than commercial MoS_2 samples (see Figure S10 in the Supporting Information). We expect that the HER activity of such HNN-MoS_2 nanostructures can be further improved by the decoration of graphene or a noble metal.[3b,22] More systematic investigations are needed for a better understanding of the improved activity of HNN-MoS_2 for photoelectrochemical water splitting.

In summary, we have demonstrated a facile synthesis of hierarchical nanosheet-based MoS_2 nanotubes with good structural stability by the anion-exchange reaction of MoO_3–EDA nanowires with S^{2-} anions at elevated temperature. The dissolution of EDA in the solvent and the concentration-gradient-driven outward diffusion of MoO_3–EDA during the anion-exchange reaction are the key factors in the formation of the hierarchical tubular structures with the retention of the 1D morphology of the starting hybrid nanowires. The photocurrent density (ca. 0.67 mA mg^{-1} at 0.6 V versus SCE) of the as-prepared hierarchical nanosheet-based MoS_2 nanotubes is 9 times higher than that of commercial MoS_2 samples. The improved activity of the hierarchical nanosheet-based MoS_2 nanotubes may be associated with their enhanced ability to absorb photons, the presence of many more active sites, and the unique hierarchical porous structure of the nanosheets. Furthermore, the as-prepared hierarchical MoS_2 nanotubes exhibit high resistance to photocorrosion. The combination of the facile synthetic procedure, the high photoelectrochemical and electrochemical activity, and the low cost of the starting materials may make the hierarchical nanosheet-based MoS_2 nanotubes one of the most promising candidates for photoelectrocatalytic and electrocatalytic HER as well as the fabrication of practical photoelectrochemical electrodes. Furthermore, the hierarchical nanosheet-based MoS_2 nanotubes may be of special interest for a variety of promising applications, including organic and industrial catalysis,[2] battery materials,[7] and hydrogen storage.[6] The extension of this simple anion-exchange strategy for the transformation of inorganic–organic hybrid nanostructures to the synthesis of other hierarchical inorganic nanotubes is under way in our research group.

Received: April 24, 2013
Published online: July 3, 2013

Keywords: anion exchange · hierarchical architectures · inorganic–organic hybrid composites · nanotubes · photoelectrochemical water splitting

[1] S. Iijima, *Nature* **1991**, *354*, 56.
[2] a) O. Y. Gutiérrez, A. Hrabar, J. Hein, Y. Yu, J. Han, J. A. Lercher, *J. Catal.* **2012**, *295*, 155; b) M. Polyakov, S. Indris, S. Schwamborn, A. Mazheika, M. Poisot, L. Kienle, W. Bensch, M. Muhler, W. Grünert, *J. Catal.* **2008**, *260*, 236; c) T. Drescher, F. Niefind, W. Bensch, W. Grünert, *J. Am. Chem. Soc.* **2012**, *134*, 18896; d) Q. Gao, C. Giordano, M. Antonietti, *Angew. Chem.* **2012**, *124*, 11910; *Angew. Chem. Int. Ed.* **2012**, *51*, 11740.
[3] a) B. Seger, A. B. Laursen, P. C. K. Vesborg, T. Pedersen, O. Hansen, S. Dahl, I. Chorkendorff, *Angew. Chem.* **2012**, *124*, 9262; *Angew. Chem. Int. Ed.* **2012**, *51*, 9128; b) Y. Hou, A. B. Laursen, J. Zhang, G. Zhang, Y. Zhu, X. Wang, S. Dahl, I. Chorkendorff, *Angew. Chem.* **2013**, *125*, 3709; *Angew. Chem. Int. Ed.* **2013**, *52*, 3621; c) W. Zhou, Z. Yin, Y. Du, X. Huang, Z. Zeng, Z. Fan, H. Liu, J. Wang, H. Zhang, *Small* **2013**, *9*, 140; d) X. Zong, H. Yan, G. Wu, G. Ma, F. Wen, L. Wang, C. Li, *J. Am. Chem. Soc.* **2008**, *130*, 7176; e) F. A. Frame, F. E. Osterloh, *J. Phys. Chem. C* **2010**, *114*, 10628; f) D. Merki, S. Fierro, H. Vrubel, X. Hu, *Chem. Sci.* **2011**, *2*, 1262; g) D. Merki, H. Vrubel, L. Rovelli, S. Fierro, X. Hu, *Chem. Sci.* **2012**, *3*, 2515.
[4] M. S. Fuhrer, J. Hone, *Nat. Nanotechnol.* **2013**, *8*, 146.
[5] M. Chhowalla, G. A. Amaratunga, *Nature* **2000**, *407*, 164.
[6] a) J. Chen, N. Kuriyama, H. Yuan, H. T. Takeshita, T. Sakai, *J. Am. Chem. Soc.* **2001**, *123*, 11813; b) L. Ye, C. Wu, W. Guo, Y. Xie, *Chem. Commun.* **2006**, 4738.
[7] a) C. Zhang, Z. Wang, Z. Guo, X. W. Lou, *ACS Appl. Mater. Interfaces* **2012**, *4*, 3765; b) L. Yang, S. Wang, J. Mao, J. Deng, Q. Gao, Y. Tang, O. G. Schmidt, *Adv. Mater.* **2013**, *25*, 1180; c) K. Chang, W. Chen, *ACS Nano* **2011**, *5*, 4720; d) Y. Liang, R. Feng, S. Yang, H. Ma, J. Liang, J. Chen, *Adv. Mater.* **2011**, *23*, 640; e) H. Liu, D. Su, R. Zhou, B. Sun, G. Wang, S. Z. Qiao, *Adv. Energy Mater.* **2012**, *2*, 970; f) X. L. Li, Y. D. Li, *J. Phys. Chem. B* **2004**, *108*, 13893.
[8] G. Ma, H. Peng, J. Mu, H. Huang, X. Zhou, Z. Lei, *J. Power Sources* **2013**, *229*, 72.
[9] a) A. Yella, M. Kappl, M. Panthöfer, W. Tremel, *Angew. Chem.* **2010**, *122*, 2629; *Angew. Chem. Int. Ed.* **2010**, *49*, 2575; b) J. Tannous, F. Dassenoy, B. Vacher, T. Le Mogne, A. Bruhacs, W. Tremel, *Tribol. Lett.* **2011**, *41*, 55; c) Y. Tian, Y. He, Y. Zhu, *Mater. Chem. Phys.* **2004**, *87*, 87; d) H. S. S. Ramakrishna Matte, A. Gomathi, A. K. Manna, D. J. Late, R. Datta, S. K. Pati, C. N. R. Rao, *Angew. Chem.* **2010**, *122*, 4153; *Angew. Chem. Int. Ed.* **2010**, *49*, 4059; e) M. Nath, A. Govindaraj, C. N. R. Rao, *Adv. Mater.* **2001**, *13*, 283.
[10] a) M. Hershfinkel, L. A. Gheber, V. Volterra, J. L. Hutchison, R. Tenne, *J. Am. Chem. Soc.* **1994**, *116*, 1914; b) Y. Feldman, E. Wasserman, D. J. Srolovitz, R. Tenne, *Science* **1995**, *267*, 222.
[11] D. H. Son, S. M. Hughes, Y. Yin, A. P. Alivisatos, *Science* **2004**, *306*, 1009.
[12] a) E. Muthuswamy, S. L. Brock, *J. Am. Chem. Soc.* **2010**, *132*, 15849; b) R. D. Robinson, B. Sadtler, D. O. Demchenko, C. K. Erdonmez, L. W. Wang, A. P. Alivisatos, *Science* **2007**, *317*, 355; c) K. Miszta, D. Dorfs, A. Genovese, M. R. Kim, L. Manna, *ACS Nano* **2011**, *5*, 7176.
[13] a) J. B. Rivest, P. K. Jain, *Chem. Soc. Rev.* **2013**, *42*, 89; b) J. Yao, S. Schachermeyer, Y. Yin, W. Zhong, *Anal. Chem.* **2011**, *83*, 402; c) Y. Liu, J. Goebl, Y. Yin, *Chem. Soc. Rev.* **2013**, *42*, 2610.
[14] a) H. Tong, Y. J. Zhu, L. X. Yang, L. Li, L. Zhang, *Angew. Chem.* **2006**, *118*, 7903; *Angew. Chem. Int. Ed.* **2006**, *45*, 7739; b) H.-W. Liang, J.-W. Liu, H.-S. Qian, S.-H. Yu, *Acc. Chem. Res.* **2013**, *46*, DOI: 10.1021/ar300272m.
[15] a) Y. Yu, J. Zhang, X. Wu, W. Zhao, B. Zhang, *Angew. Chem.* **2012**, *124*, 921; *Angew. Chem. Int. Ed.* **2012**, *51*, 897; b) X. Wu, Y. Yu, Y. Liu, Y. Xu, C. Liu, B. Zhang, *Angew. Chem.* **2012**, *124*, 3265; *Angew. Chem. Int. Ed.* **2012**, *51*, 3211.
[16] a) Y. Hou, F. Zuo, A. Dagg, P. Feng, *Nano Lett.* **2012**, *12*, 6464; b) Y. Hou, F. Zuo, A. Dagg, P. Feng, *Angew. Chem.* **2013**, *125*, 1286; *Angew. Chem. Int. Ed.* **2013**, *52*, 1248; c) A. Kongkanand, R. M. Domínguez, P. V. Kamat, *Nano Lett.* **2007**, *7*, 676; d) S. Chen, J. Duan, M. Jaroniec, S. Z. Qiao, *J. Mater. Chem. A* **2013**, DOI: 10.1039/C3A00133D.
[17] Q. Gao, S. Wang, H. Fang, J. Weng, Y. Zhang, J. Mao, Y. Tang, *J. Mater. Chem.* **2012**, *22*, 4709.
[18] C. Zhang, H. B. Wu, Z. Guo, X. W. Lou, *Electrochem. Commun.* **2012**, *20*, 7.
[19] a) Y. Feldman, V. Lyakhovitskaya, R. Tenne, *J. Am. Chem. Soc.* **1998**, *120*, 4176; b) Z. Chen, D. Cummins, B. N. Reinecke, E. Clark, M. K. Sunkara, T. F. Jaramillo, *Nano Lett.* **2011**, *11*, 4168.
[20] a) E. Benavente, M. A. Santa Ana, F. Mendizábal, G. González, *Coord. Chem. Rev.* **2002**, *224*, 87; b) K. K. Kam, B. A. Parkinson, *J. Phys. Chem.* **1982**, *86*, 463.
[21] T. F. Jaramillo, K. P. Jørgensen, J. Bonde, J. H. Nielsen, S. Horch, I. Chorkendorff, *Science* **2007**, *317*, 100.
[22] a) J. Kim, S. Byun, A. J. Smith, J. Yu, J. Huang, *J. Phys. Chem. Lett.* **2013**, *4*, 1227; b) Y. Li, H. Wang, L. Xie, Y. Liang, G. Hong, H. Dai, *J. Am. Chem. Soc.* **2011**, *133*, 7296.